Literatur

1. *P. John,* Schweißen im Behälter- und Apparatebau. DVS-Berichte *84* (1984) 4–7.
2. *J. Hessel, D. Hausdörfer, B. Kempe,* Zum Einfluß von oxidierenden, oberflächenaktiven und quellenden Medien auf Schweißverbindungen aus PE-HD, IIW-Doc. (1984) 453–484.
3. *B. Kempe,* Prüfmethoden zur Ermittlung des Verhaltens von Polyolefinen bei der Einwirkung von Chemikalien. Zeitschriften für Werkstofftechnik *15* (1984) 157–172.
4. Beiheft Nr. 22 zur Zeitschrift Müll und Abfall 1985, Herausg. *F. W. Knipschild,* mit Beiträgen von *K. Stief, G. Friesecke, D. Schnepel, W. Kanning, L. Glück* und *J. Zöhren, A. Schlütter, F. W. Knipschild, R. Taprogge, G. Menges* und *E. Schmachtenberg, H. August* u. *R. Tatzky, L. Glück* u. *G. Poschet, Ch. Hostettler, D. Nagel, H. J. Vock, K. Ungruh, C. A. Günther, H. Kroh:* S. 25–28.
5. *J. Hessel, E. Schweiger,* Schäl- und Zugversuche an überlappt geschweißten HDPE-Folien. Nichtveröffentlichter Versuchsbericht der Hoechst AG, 1980.
6. Deutscher Verband für Schweißtechnik e.V., Merkblatt DVS 2203, Teil 4 (1986). Prüfen von Schweißverbindungen aus Kunststoff, Zeitstand-Zugversuch.
7. *G. Diedrich, E. Gaube,* Schweißverfahren für Rohre und Platten aus Hart-Polyethylen. Kunststoffe *60* (1970) 74–80.
8. *P. John, J. Hessel, E. Gaube,* Eine Neuentwicklung auf dem Gebiet des Extrusionsschweißens. Kunststoffe *75* (1985) 11–13.

Anschrift: Dr.-Ing. *J. Hessel* und Ing. (grad.) *P. John,* Hoechst Aktiengesellschaft, Abt. Werkstofftechnik, Postfach 800320, 6230 Frankfurt/M. 80.

[T233]

Stress Intensity Factors of Partly Circumferential Surface Cracks at the Outer Wall of a Pipe

H. Grebner

By means of the finite element method stress intensity factors were calculated for partly circumferential surface cracks at the outer wall of a pipe. The crack shape considered can be described as curved rectangular shape. The cracks considered have crack depths between 20 and 80 percent of the wall thickness of the pipe and crack lengths (defined by the angle of circumference φ) between $\varphi = 10°$ and $\varphi = 60°$. The pipe is loaded by a constant axial tensile stress σ_0 (equal to 136 Nmm^{-2} in the numerial calculations), and the wall thickness to inner radius ratio of the pipe was chosen to 0.1. A wall thickness of 20 mm was used for the numerical calculations.

Spannungsintensitätsfaktoren für teilweise umlaufende Oberflächenumfangsrisse an der Außenwand eines Rohres

Mit Hilfe der Finite-Element-Methode wurden Spannungsintensitätsfaktoren berechnet für teilweise umlaufende Umfangsoberflächenrisse an der Außenwand eines Rohres. Die untersuchte Rißform läßt sich als gebogenes Rechteck bezeichnen. Die betrachteten Risse weisen Rißtiefen zwischen 20 und 80% der Rohrwandstärke auf und haben Rißlängen (definiert durch den Winkel φ in Umfangsrichtung) zwischen $\varphi = 10°$ und $\varphi = 60°$. Das Rohr ist durch eine konstante axiale Zugspannung σ_0 (gleich 136 Nmm^{-2} bei den numerischen Rechnungen) beansprucht, und das Verhältnis Wandstärke – zu – Innenradius des Rohres wurde zu 0.1 festgelegt. Für die numerischen Rechnungen wurde eine Wandstärke von 20 mm verwendet.

1 Introduction

Welded joints in pressurized piping components may contain faults, which eventually are the reason for the formation of surface cracks. The welded joints are often arranged in circumferential direction, so that it is necessary to study also circumferential cracks in spite of the fact, that these mostly are loaded less than axial surface cracks.

To make predictions of the fatigue crack growth and the stability behaviour it is necessary to have knowledge of the stress intensity factors in the actual case. For axially orientated cracks *Newman* and *Raju* [1] have given solutions for cracks at the inner and outer wall of the pipe. Partly circumferential cracks at the inside of a pipe have been treated by *Morawietz, Mattheck* and *Munz* [2]. In this paper similar cracks are considered, located at the outer wall of the pipe. Crack geometry and notations are shown in *Fig. 1.*

2 Finite Element Models and Calculations

By means of the program SUPERNET [3] several three dimensional finite element structures were generated, having on principle the same arrangement. Starting with one crack geometry the super structure of this crack was built up in such a way, that all other nets could be gained from the first one by only slight modifications. In this way finite element structures were generated for cracks with a crack depth to wall thickness ratio a/t of 0.2, 0.4, 0.6 and 0.8 and with a crack angle of 10, 20, 30 and 60 degrees. The geometrical parameters of the pipe were chosen to $R_i = 200$ mm, $t = 20$ mm and the pipe length $l = 1000$ mm. *Figs. 2* to *5* present hidden-line plots for some examples. The largest structures consist of 566 elements with 5670 nodal points and nearly 8500 unknowns. For symmetry reasons only a quarter of the pipe has to be modelled.

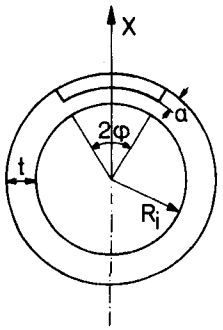

Fig. 1. Circumferential surface crack – geometry and notations.

Abb. 1. Umfangsoberflächenriß – Geometrie und Bezeichnungen.

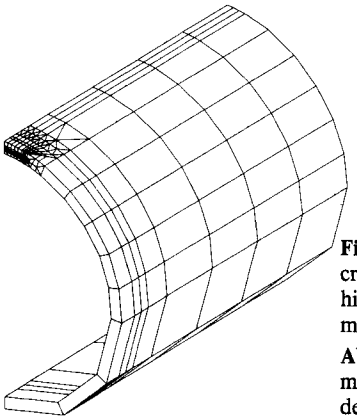

Fig. 2. Circumferential surface crack with a/t = 0.6 and φ = 10° – hidden line plot of the finite element net.

Abb. 2. Umfangsoberflächenriß mit a/t = 0.6 and φ = 10° – Hidden-Line-Plot der FE-Struktur.

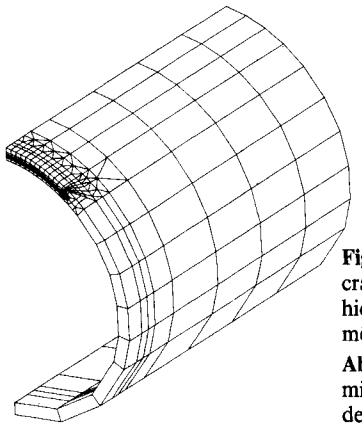

Fig. 3. Circumferential surface crack with a/t = 0.4 and φ = 30° – hidden line plot of the finite element net.

Abb. 3. Umfangsoberflächenriß mit a/t = 0.4 and φ = 30° – Hidden-Line-Plot der FE-Struktur.

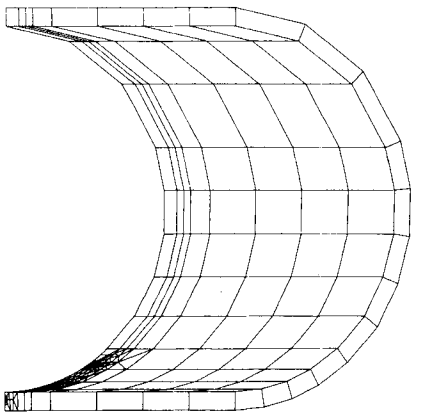

Fig. 4. Circumferential surface crack with a/t = 0.6 and φ = 30° – hidden line plot of the finite element net.

Abb. 4. Umfangsoberflächenriß mit a/t = 0.6 und φ = 30° – Hidden-Line-Plot der FE-Struktur.

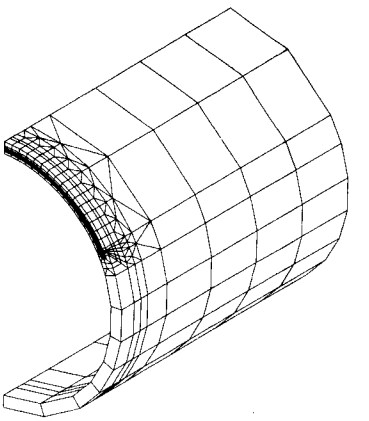

Fig. 5. Circumferential surface crack with a/t = 0.6 and φ = 60° – hidden line plot of the finite element net.

Abb. 5. Umfangsoberflächenriß mit a/t = 0.6 and φ = 60° – Hidden-Line-Plot der FE-Struktur.

To minimize computing time in the most cases the substructure technique was applied. Thereby the refined region surrounding the crack was used as a substructure and the rest of the pipe as another one. Furthermore, in order to get an appropriate modelling of the stress singularity at the crack front, quarter point elements were used to build up the crack front.

The calculations were carried out using the finite element program ASKA [4] and assuming E = 207 000 Nmm^{-2} and ν = 0.3, respectively. The pipe was loaded by a constant axial tensile stress σ_0 = 136 Nmm^{-2}, which was applied at the crack free end of the pipe.

3 Results and Discussion

Fig. 6 shows some notations, which are introduced for the presentation of the results. For the example of a crack with a/t = 0.6 and φ = 30° *Figs. 7* and *8* present the calculated crack opening displacement u_z in depth direction (from point A to point C in Fig. 6) and following the outer surface of the pipe (from point C to point B in Fig. 6). By means of the extrapolation technique stress intensity factors were evaluated at different points of the crack front using the corresponding crack opening displacements. For all cracks under consideration the stress-intensity factors K_A at point A of Fig. 6 and K_B, respectively, at point B of Fig. 6 were calculated. The values gained are given in *Table 1.*

For several cracks stress intensity factors were evaluated additionally at other points of the crack front (with the exception of point D in Fig. 6, where a meaningful definition of K is

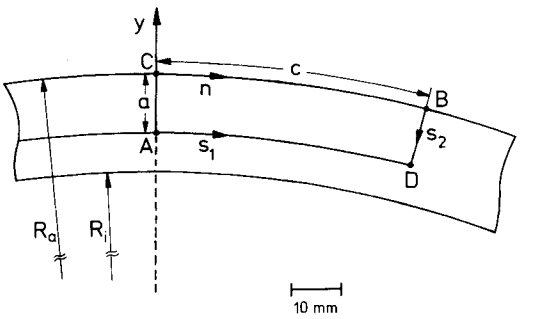

Fig. 6. Circumferential surface crack – notations concerning the presentation of results.

Abb. 6. Umfangsoberflächenriß – Bezeichnungen zur Darstellung der Ergebnisse.

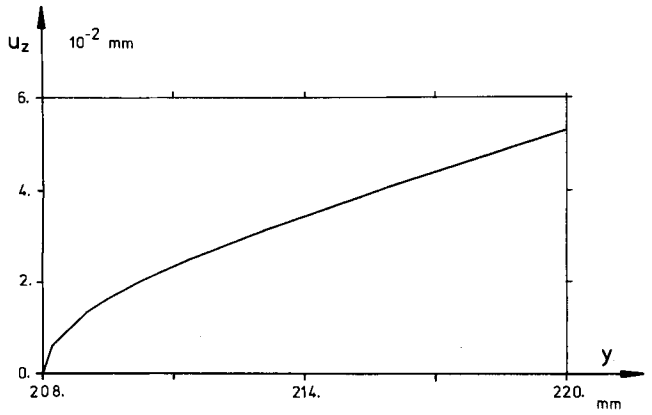

Fig. 7. Circumferential surface crack with a/t = 0.6 and φ = 30° – crack opening displacement u_z in depth direction (from point A to point C in Fig. 6).

Abb. 7. Umfangsoberflächenriß mit a/t = 0.6 und φ = 30° – Rißuferverschiebung u_z in Tiefenrichtung (von Punkt A zum Punkt C in Abb. 6).

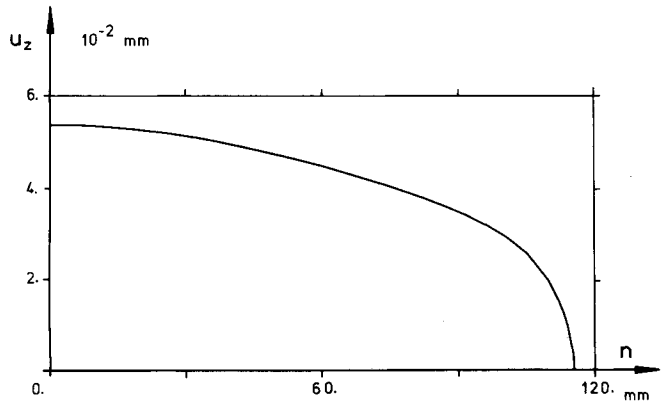

Fig. 8. Circumferential surface crack with a/t = 0.6 and φ = 30° – crack opening displacement u_z at the outer wall of the pipe (from point C to point B in Fig. 6).

Abb. 8. Umfangsoberflächenriß mit a/t = 0.6 and φ = 30° – Rißuferverschiebung u_z längs der äußeren Rohrwand (von Punkt C nach B in Abb. 6).

Table 1. Results of the stress intensity factor evaluation.

a/t	φ	K_A/Nmm$^{-3/2}$	K_B/Nmm$^{-3/2}$
0.2	10°	576	443
0.2	20°	592	443
0.2	30°	596	435
0.2	60°	598	450
0.4	10°	960	780
0.4	20°	1097	794
0.4	30°	1110	805
0.4	60°	1122	773
0.6	10°	1167	1050
0.6*	20°	–	–
0.6	30°	1842	1150
0.6	60°	1904	1120
0.8	10°	1245	1250
0.8	20°	2220	1770
0.8	30°	2770	1785
0.8	60°	3100	1630

* Not calculated.

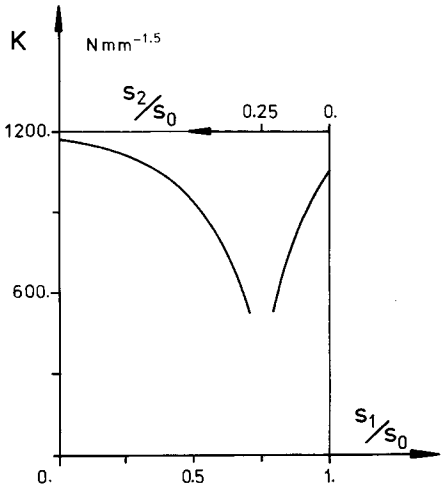

Fig. 9. Circumferential surface crack with a/t = 0.6 and φ = 10° – variation of the stress intensity factor along the crack front (explanation of s_1 and s_2 in Fig. 6).

Abb. 9. Umfangsoberflächenriß mit a/t = 0.6 und φ = 10° – Verlauf des Spannungsintensitätsfaktors längs der Rißfront (Erläuterung von s_1 und s_2 in Abb. 6).

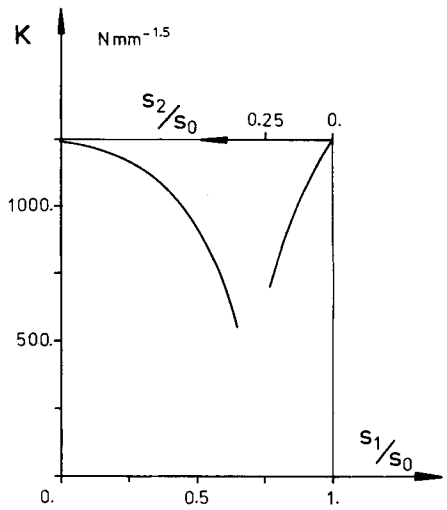

Fig. 10. Circumferential surface crack with a/t = 0.8 and φ = 10° – variation of the stress intensity factor along the crack front.

Abb. 10. Umfangsoberflächenriß mit a/t = 0.8 und φ = 10° – Verlauf des Spannungsintensitätsfaktors längs der Rißfront.

not possible). Some examples of these calculations are given in *Figs. 9* to *11* for cracks with a/t = 0.6 and φ = 10°, a/t = 0.8 and φ = 10° as well as a/t = 0.6 and φ = 30°. Thereby the stress intensity factors are shown as functions of the crack front coordinates s_1 and s_2 as introduced in Fig. 6 (s_0 is the half length of the crack front).

As a basis for the derivation of weight functions, which shall be done in a further paper, the maximum values of the axial crack opening displacement are needed. These are given in *Table 2.*

Furthermore, *Figs. 14* and *15* show geometry functions F_A and F_B at the points A and B of the crack front, given by the well known relation

$$K = \sigma_0 \sqrt{\pi a}\, F(a/t)$$

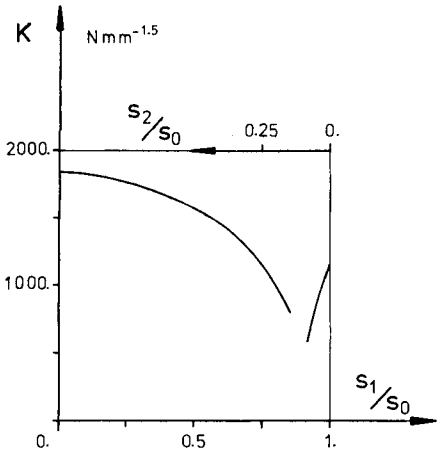

Fig. 11. Circumferential surface crack with a/t = 0.6 and φ = 30° – variation of the stress intensity factor along the crack front.

Abb. 11. Umfangsoberflächenriß mit a/t = 0.6 und φ = 30° – Verlauf des Spannungsintensitätsfaktors längs der Rißfront.

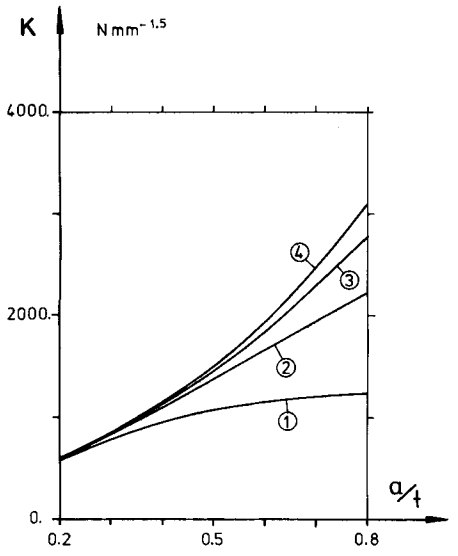

Fig. 12. Stress intensity factors K_A at the deepest crack point as functions of a/t (1: φ = 10°, 2: φ = 20°, 3: φ = 30°, 4: φ = 60°).

Abb. 12. Spannungsintensitätsfaktoren K_A am tiefsten Rißpunkt in Abhängigkeit von a/t (1: φ = 10°, 2: φ = 20°, 3: φ = 30°, 4: φ = 60°).

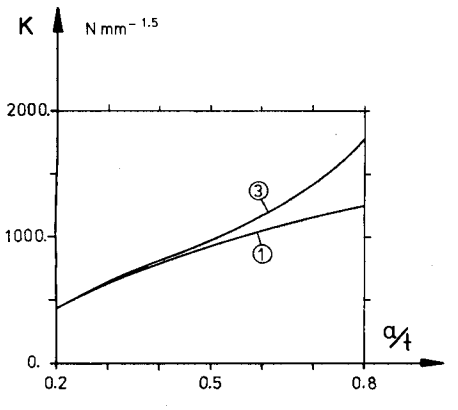

Fig. 13. Stress intensity factors K_B at the surface points as functions of a/t (1: φ = 10°, 3: φ = 30°).

Abb. 13. Spannungsintensitätsfaktoren K_B an den Oberflächenpunkten in Abhängigkeit von a/t (1: φ = 10°, 3: φ = 30°).

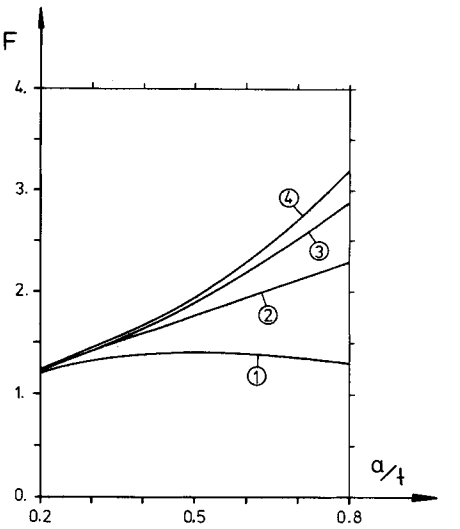

Fig. 14. Geometry functions F_A at the deepest crack point as functions of a/t (1: φ = 10°, 2: φ = 20°, 3: φ = 30°, 4: φ = 60°).

Abb. 14. Geometriefunktionen F_A am tiefsten Rißpunkt in Abhängigkeit von a/t (1: φ = 10°, 2: φ = 20°, 3: φ = 30°, 4: φ = 60°).

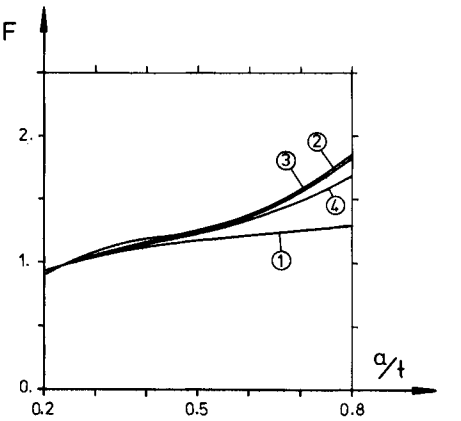

Fig. 15. Geometry functions F_B at the surface points as functions of a/t (1: φ = 10°, 2: φ = 20°, 3: φ = 30°, 4: φ = 60°).

Abb. 15. Geometriefunktionen F_B an den Oberflächenpunkten in Abhängigkeit von a/t (1: φ = 10°, 2: φ = 20°, 3: φ = 30°, 4: φ = 60°).

Table 2. Calculated maximum axial crack opening displacements.

a/t		$u_{Zmax}/10^{-3}$ mm
0.2	10°	7.67
0.2	20°	7.92
0.2	30°	7.95
0.2	60°	7.98
0.4	10°	19.40
0.4	20°	22.57
0.4	30°	23.27
0.4	60°	23.72
0.6	10°	32.53
0.6*	20°	–
0.6	30°	53.78
0.6	60°	55.16
0.8	10°	43.63
0.8	20°	88.27
0.8	30°	111.50
0.8	60°	122.70

* Not calculated.

By means of the geometry functions stress intensity factors may be calculated for other loadings and pipe geometries for the crack parameters considered, presuming only that the wall thickness to inner radius ratio of the pipe is 1 : 10 and that the axial stress in the uncracked pipe remains constant through the wall.

Loading cases which generate stress gradients in the uncracked pipe – as for example thermo-shock problems – cannot be treated with the results presented in this paper, but by means of the weight functions method, which will be available soon.

References

1. *J. Newman, I. Raju,* An empirical stress intensity factor equation for the surface crack. Eng. Fract. Mech. *15* (1981) 185–192.
2. *P. Morawietz, C. Mattheck, D. Munz,* Stress intensity factor of partly circumferential surface cracks at the inside of a pipe loaded arbitrarily. Transactions of the 8th International Conference on Structural Mechanics in Reactor Technology, Brussels, Belgium (1985) G 5/6.
3. *K. E. Buck, U. von Bodisco, K. Winkler,* SUPERNET generation and presentation – user's guides. BBC Mannheim.
4. ASKA Part I – Linear static analysis, user's reference manual. ISD-report 73, Stuttgart (1971).

Anschrift: Dr. *Hans Grebner,* Brown, Boveri & Cie AG, 6800 Mannheim.

[T 226]

On the Effect of Temperature Cycling on the Coating of a Pack Aluminized Low Alloyed Steel (13 CrMo 44)

Th. Uihlein, G. Eggeler and H. J. Maier

Coated pack aluminized low alloyed steels are known for their good resistance against high temperature corrosion up to 700 °C, where diffusion stability is still sufficient. In typical high temperature applications, coating and substrate are subjected to thermal fatigue. In this study the metallurgical stability of a coated, pack aluminized, low alloyed steel is reported. The specimens were cyclically quenched from 700 °C to room temperature or liquid nitrogen temperature respectively, to assess the importance of thermal shock severity on the kinetic of degradation. In particular, crack initiation and growth were studied. The dependence of microcrack densities upon numbers of cycles, cooling rates and specimen geometry is reported.

Zum Einfluß von Temperaturwechseln auf Pulveraluminierschutzschichten auf niedriglegiertem Stahl (13 CrMo 44)

Durch Pulveraluminieren von niedriglegiertem Stahl kann gute Beständigkeit gegen Hochtemperaturkorrosion bis zu 700 °C erreicht werden, ohne daß Diffusionsprozesse schon zu einer Verarmung von Aluminium in der Probenoberfläche führen. Im normalen Hochtemperatureinsatz ist die Schutzschicht auch Temperaturwechseln unterworfen. In dieser Untersuchung wird berichtet, wie Pulveraluminierschutzschichten auf Temperaturwechsel zwischen 700 °C und Raumtemperatur bzw. Temperatur des flüssigen Stickstoffs reagieren. Neben Rißbildung und -wachstum wird die Abhängigkeit der Mikrorißdichte von Zyklenzahl, Abkühlgeschwindigkeit und Probengeometrie beschrieben.

1 Introduction

It is well known that pack aluminized steels show good resistance against high temperature corrosion in atmospheres containing sulphur and carbon [1–4]. The build up of pack aluminized coatings on steels has been described in literature [7, 13, 14]. Thermogravimetric studies in H_2/H_2S gas mixtures were performed [5, 6] to describe and understand the slow sulfidation kinetics of such coatings. Corrosion attack [5, 6] and loss of aluminium in the coating due to interdiffusion processes [7] were found to be negligible up to 700 °C. It remains to be proven, that such coatings can withstand thermal fatigue conditions. Although thermal cycling is recognized to be a severe problem for all kinds of high temperature coatings [8–11], still little information has been published about the nature of the damage in the coating during thermal cycling. The purpose of the present paper is to investigate the effect of thermal fatigue on the coating of a pack aluminized low alloyed steel under well defined experimental conditions. The aim of this metallurgical study was to shed some light on the factors that influence degradation and cracking behavior of a the coating. To achieve this goal, a pack aluminized steel was cyclically quenched between 700 °C and room temperature or 700 °C and liquid nitrogen temperature, to adjust two well defined states of thermal stresses. Crack initiation and growth were in the focus of interest. The dependence of microcrack density on number of cycles, stress state and specimen geometry is reported.